Effect of Si on the SLM processability of IN738LC

R. Engeli*†, T. Etter*, F. Geiger*, A. Stankowski*, K. Wegener†

* ALSTOM (Switzerland) Ltd, Brown-Boveri Str. 7, 5400 Baden, Switzerland
† Institute of machine tools and manufacturing (IWF), ETH Zürich, Switzerland

REVIEWED

Abstract

Selective laser melting of high gamma-prime strengthened superalloys such as IN738LC is of interest in stationary gas turbine applications. Differences have been obtained for the hot cracking susceptibility of different powder batches during SLM processing and indications were found that also minor elements influence the SLM processability. By processing a specific powder batch blended by different amounts of pure silicon, the detrimental effect of this element during SLM could be shown. Therefore, the control of this minor element is crucial to decrease the hot cracking tendency and can extend the SLM processing window of this alloy.

Introduction

Selective Laser Melting (SLM) is an emerging additive manufacturing method for the fabrication of complex parts out of metal powder. The process consists of repeated application of thin (20-60 μm) powder layers which are subsequently densified by a scanning laser beam according the layer information from a sliced 3D model. This process provides new possibilities in the design of complex components and is therefore of large interest for applications in stationary and aeronautical gas turbines.

For such applications, high temperature alloys such as nickel based superalloys are used for components in the hot gas path of gas turbines. The high strength of this alloy class is based on a strong solid solution strengthening of the fcc γ-Ni matrix and on precipitation hardening by ordered, coherent intermetallic phases such as γ'-Ni$_3$(Al,Ti) or γ''-Ni$_3$Nb. Further strengthening is provided by solid solution strengthening of the intermetallic phases and grain boundary strengthening with carbides, boron and zirconium. This alloy class is known to be difficult to process by SLM and many alloys are susceptible to severe hot cracking as reported by Gasser et al. [1] and Kelbassa et al. [2] for the alloy MarM247, by Uhlmann and Urban [3] for René80 and by Carter et al. [4,5] for CM247LC. As shown by Tomus et al. [6], this hot cracking problematic is not limited to γ'-strengthened alloy, but also exists for the solid solution strengthened alloys such as Hastelloy X. In their work, Tomus et al. showed that the minor elements Mn and Si affect the hot cracking susceptibility.

In a recent work of the authors [7], the SLM processability of various batches of IN738LC was assessed and it was found that also for this γ'-strengthened alloy, the different batches strongly differ in their hot cracking susceptibility. Though being within the original specification for IN738LC given in Table 2, strong variations in the crack densities up to factor of ten were found in the different batches (see Figure 1). Indications were found that the minor element Si has a strong effect on cracking susceptibility even on a very low content level, but an unambiguous identification of the critical elements was not possible due to the large amount of varying elements compared to the number of powder batches which were investigated.

It is already known from conventional welding research that some elements such as boron, sulfur or phosphorous strongly affect hot cracking even on ppm level [8]. To unambiguously identify the influence of the different elements, either a statistical evaluation of a large number of different batches (>> number of varying elements) is required or test series must be performed where only the content of specified elements varies while the others are kept constant. The latter might be achieved by atomization of different batches from a common master melt with different additions of a specific element. However, due to the high atomization cost for such alloys both of these ways are very cost intensive.
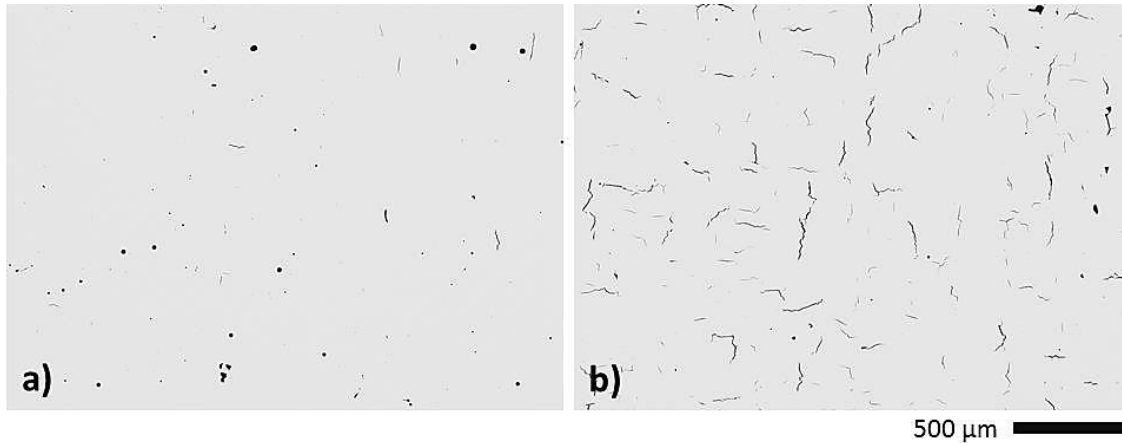
Figure 1: Representative microsection of a SLM made sample processed under equal conditions from a) a 'good' and b) a 'bad' IN738LC powder batch.

Another approach to assess the influence of minor elements is to blend a powder batch with low amounts of a second powder enriched with the element to be investigated. Such an approach is more versatile and cost effective, as it allows the preparation of various compositions from the same source powders. However, it requires that both components are completely melted and well homogenized during the SLM process. In a first step, the homogenization of a simple powder blend consisting of 50% IN738LC and 50% CM247LC powder during SLM was assessed. These alloys were chosen because they can be well distinguished by backscatter electron microscopy and by EDX mapping, allowing an easy investigation of the homogenization efficiency during SLM. In a second step, this blending approach was applied to investigate the effect of Si on the processability of IN738LC.

Experimental procedure

In the predecessor experiment, the capability of the SLM process to homogenize a powder blend was assessed by the investigation of samples made of a 50wt%:50wt% powder blend of IN738LC and CM247LC. Both powders were gas atomized and mainly consist of spherical particles with a D50 of 18 µm (IN738LC) and 33 µm (CM247LC) respectively. The chemical composition of the source powders is given in Table 1. To prepare the powder mixture, 500g of each powder was added to a plastic bottle and blended in a tumbling mixer for 20 minutes.

To investigate the effect of Si on the SLM processability of IN738LC, four different blends of IN738LC powder with A) 0 wt-%, B) 0.05 wt-%, C) 0.125 wt-% and D) 0.2 wt-% pure Si powder were prepared. The IN738LC powder showed a spherical morphology with a D50 of 36 µm. An irregular shaped, fine Si powder with a D50 of 3.6 µm was used for blending. The chemical composition of the two source powders is shown in Table 2. After adding the appropriate amount of Si powder to the IN738LC powder, the blends were homogenized in a tumbling mixer for 10 minutes and further de-agglomerated by ball milling for 120 min. To ensure equal conditions, the same procedure was also applied to the pure IN738LC powder batch.

In order to cope with the low amount of powder available, a low volume insert developed by Inspire AG was used. From each powder blend, three cuboids with dimensions 15x10x15 mm were prepared under equal conditions using a parameter set developed by Rickenbacher et. al. [9] for IN738LC using a layer thickness of 30 µm. A crosswise alternating island based scan strategy was applied with scan direction ±45° to the edges of the samples. To investigate the crack surface, a special specimen geometry was fabricated which is shown in Figure 2. The specimen was designed such that it can be easily cleaved by using a bench vise. For this specimen, the same process parameters are used, but a bidirectional scan strategy was applied as explained in Figure 2. This set-up allows the investigation of the surface of both cracks running parallel and perpendicular to the weld lines.
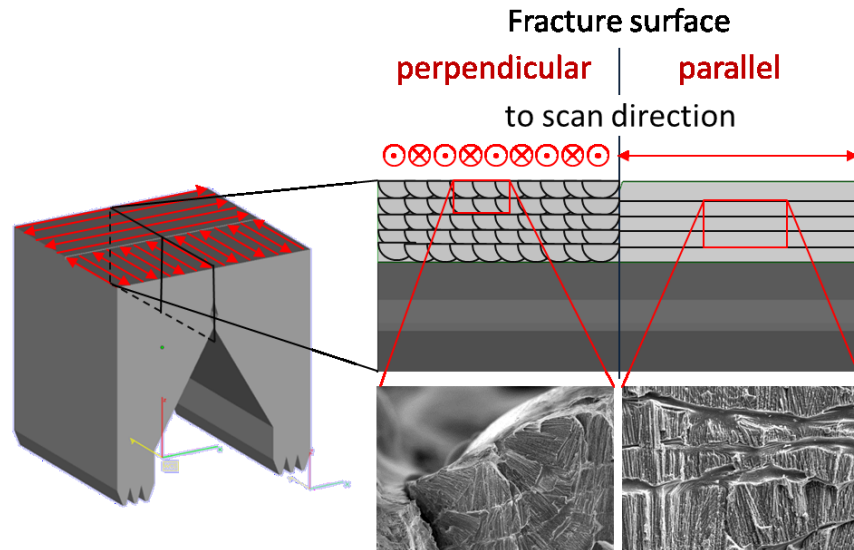
Figure 2: Schematic of the test geometry used to investigate the crack surfaces. A bi-directional scan strategy is used where the scan vectors on one side of the specimen run parallel and on the other side perpendicular to the later fracture plane. After forced fracture of the samples, the crack surface of cracks running parallel and perpendicular to the scan line can be investigated on the corresponding side of the specimen.

For metallographic analysis, two xy-microsections perpendicular to the build-up direction were prepared from each sample by grinding with a 150 grit disk (corundum) followed by polishing with 15 µm, 9 µm, 6 µm, 3 µm, and 1 µm diamond suspension. The porosity and the crack density were evaluated by quantitative image analysis using a plugin created by the first author for the software ImageJ (http://imagej.nih.gov/ij/, [10]). For each sample, 8 images with 50x magnification were evaluated. The porosity, the crack density and the corresponding uncertainties (95%) reported in this work were calculated from the average values determined for the three samples of each powder batch. A Tescan MIRA3 XMU FEG-SEM equipped with an AZtecEnergy EDX system from Oxford Instruments, operated at 20kV and with a nominal beam current of roughly 1 nA, was used for the investigation of polished microsections and EDX mapping. All other SEM images were made with a JEOL JSM-6010LA scanning electron microscope. Thermodynamic properties such as solubility limits and melting temperature were calculated with the software ThermoCalc V4 using the database NIDATA V4.

Results & Discussion

To assess the capability of the SLM process to homogenize powder blends, specimen prepared out of a 50wt-% IN738LC:50wt% CM247LC powder blend were investigated by backscatter electron (BSE) microscopy and EDX mapping. These two alloys differ strongly in several elements and can therefore be well distinguished by their z-contrast in the BSE images or by EDX mapping the Cr-Kα signal. In Figure 3, such a BSE image and an EDX map from a polished microsection of a SLM processed sample is shown.

Table 1: Chemical composition of the predecessor powders and of theoretic and measured (EDX) composition of samples processed out of the IN738LC/CM247LC powder blend.

			Ni	Cr	Co	Mo	W	Ta	Al	Ti	Hf	C	B	Zr	Nb	Fe	O$_2$	N$_2$
									[wt-%]								[wt-ppm]	
Predecessor powder	IN738LC	Supplier	bal.	16.2	8.6	1.8	2.7	1.7	3.5	3.3		0.14	0.011	0.023	0.92	0.82	400*	9*
	CM247LC	Supplier	bal.	8.0	9.1	0.5	9.9	3.2	5.6	0.7	1.3	0.06	0.013	0.009		0.05	145*	117*
50/50 mixture		calculated	bal.	12.1	8.8	1.1	6.3	2.5	4.6	2.0	0.7	0.10	0.012	0.016	0.46	0.43	273	63
Powder blend		EDX	58.9	12.3	8.9	1.3	7.1	2.9	4.7	2.1	0.5				0.50	0.42		

* LECO analysis

The slight contrast visible in the BSE images originates from channeling effects due to different grain orientations. However, no evidence for incomplete solution of the different powder particles was found in the investigated microsection. This is supported by the EDX map of the Cr-Kα signal which shows a very uniform distribution of the element. For the given process conditions, the mixing effect within the 100-200 µm broad melt pool is strong enough to homogenize the powder blend despite the rather large particles ranging between 8

to 35 μm for IN738LC and 11 to 57 μm for CM247LC. The large mixing effect might be caused by strong Marangoni convection within the melt pool which can be in the range of several meters per seconds [11,12]. As shown in Table 1, the resulting chemical composition obtained by EDX analysis matches well the expected composition calculated from the composition of the source materials.
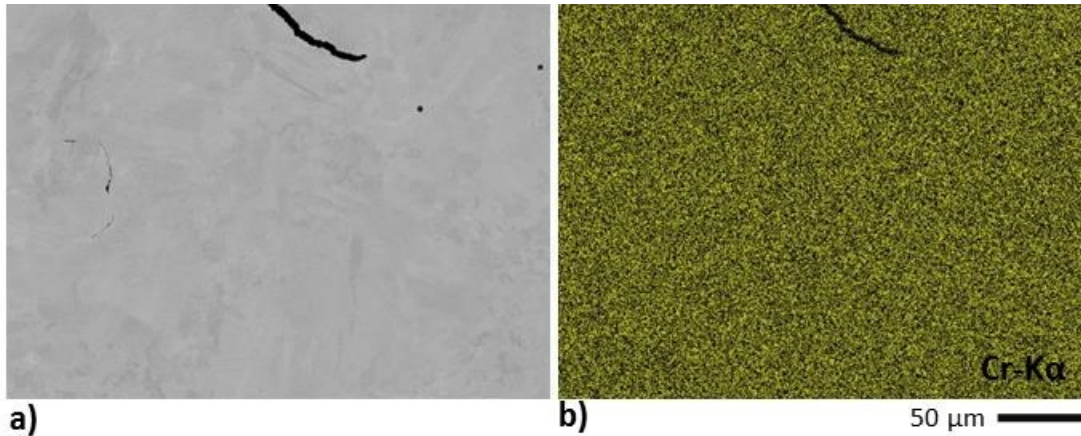

Figure 3: a) Backscatter electron microscopy image and b) EDX map for Cr-Kα of a polished microsection of a SLM processed sample from a blended IN738LC/CM247LC powder mixture.

The findings from this preliminary experiment encourage the assumption that the effects of alloying elements on SLM processing can be investigated by processing powder blends. This approach will have its limitations, e.g. when blending powders with very different melting points or using different process conditions resulting in other melt pool dynamics. Also the solubility of the elements in the matrix can be critical, even though the rapid solidification occurring in the SLM process might extend the solubility limits. These limits must be investigated in a future work.

Based on this promising result, the powder blending approach was applied to verify the detrimental effect of Si found in the author's prior work [7]. Four blends of IN738LC with 0, 0.05, 0.125 and 0.2 wt-% Si powder were prepared and investigated. The expected chemical composition of the blend can be found in Table 2. The element of interest for this investigation, silicon, has a melting point of 1414°C, only around 75°C higher than the liquidus of IN738LC. The maximum solubility of Si in pure Ni is around 1.5 wt-%, considerably higher than the range to be investigated which is below 0.2 wt-%. Based on these two considerations, it is expected that a good homogenization should also be obtained for powder blends with Si.

Table 2: Chemical composition of the used powders used to investigate the effect of Silicon on SLM processability. In the first two rows, the nominal composition of IN738LC according the technical datasheet "Alloy IN-738LC: Technical data" [13] is shown. The next two rows show the chemical composition of the source powders according to the supplier's datasheets. The four last rows show the expected composition of the blended powder mixtures A-D as calculated from the source powder compositions. All values are given in mass percent.

|		Ni	Cr	Co	Mo	W	Ta	Al	Ti	Nb	C	B	Zr	Si	O₂	N₂
Nominal IN738LC	*min.*	bal.	15.7	8	1.5	2.4	1.5	3.2	3.2	0.6	0.09	0.007	0.02	-	-	-
	max.		16.3	9	2	2.8	2	3.7	3.7	1.1	0.13	0.012	0.08	0.3	-	-
Source materials	*IN738LC powder*	bal.	16.2	8.6	1.7	2.8	2	3.5	3.3	0.75	0.095	0.01	0.016	0.018	0.0073	0.0057
	Si powder	-	-	-	-	-	-	-	-	-	0.1	-	-	98.7	1.2	-
Calculated compositions	**A:** 0 wt-% Si	bal.	16.2	8.6	1.7	2.8	2.0	3.5	3.3	0.75	0.095	0.010	0.016	0.018	0.0073	0.0057
	B: 0.05 wt-% Si		16.2	8.6	1.7	2.8	2.0	3.5	3.3	0.75	0.095	0.010	0.016	0.067	0.0079	0.0057
	C: 0.125 wt-% Si		16.2	8.6	1.7	2.8	2.0	3.5	3.3	0.75	0.095	0.010	0.016	0.141	0.0088	0.0057
	D: 0.2 wt-% Si		16.2	8.6	1.7	2.8	2.0	3.5	3.3	0.75	0.095	0.010	0.016	0.215	0.0097	0.0057
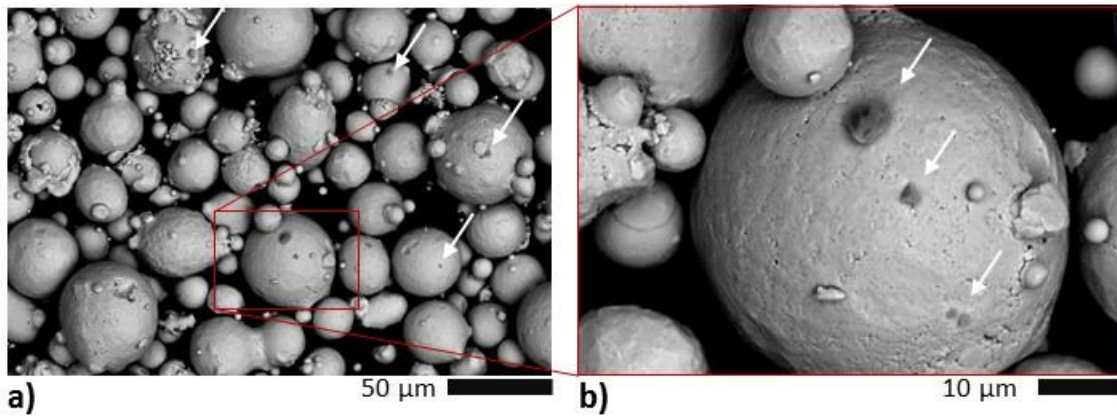
Figure 4: Backscatter electron images of IN738LC powder blended with 0.05% pure Si powder. As in the other blends, the silicon particles (marked with arrows) are well distributed and adhere to the surface of the larger IN738LC particles.

Because of the low Si contents to be investigated, a very fine Si powder with a D50 of 3.6 μm was used to get a homogenous powder mixture. Assuming that the particles of the two powders all had a uniform size corresponding to their D50 value, a rough estimate of the number fraction of Si particles in the different blends can be calculated using the bulk densities of IN738LC (8.1 g/ccm) and Si (2.33 g/ccm). This rough estimation results in number fractions of Si particles in the blends between 63% for the 0.05 wt-% blend and 87% for the 0.2 wt-% blend. For all blends, more Si particles than Ni particles are present which should favor a good homogenization during SLM. In Figure 4, a BSE image of the 0.05-wt% Si powder blend after de-agglomeration by ball-milling is shown. It can be observed that the Si particles are well distributed within the powder blend.
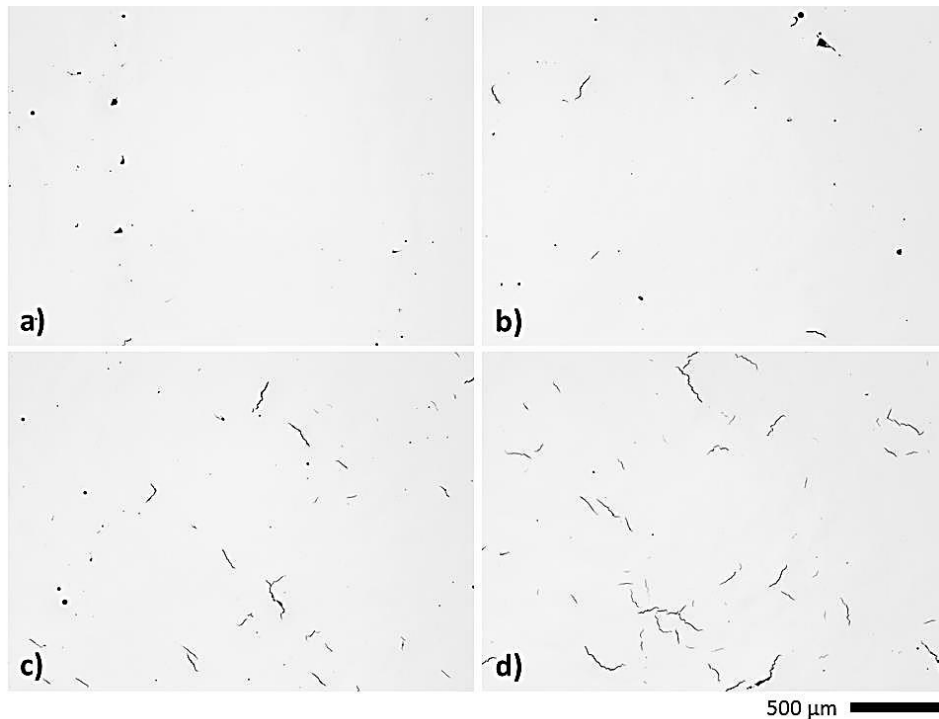

Figure 5: Representative microsections of SLM processed samples made of IN738LC blended with a) 0%, b) 0.05%, c) 0.125%, d) 0.2% Si powder.

The evaluation of the polished microsections showed a strong increase of the crack density with increasing Si powder fraction as shown in Figure 5. The results from the quantitative image analysis are given in Figure 6. While the porosity is at low values around 0.1% for all blends, the crack density is increasing from around 0.1 mm/mm2 for the pure IN738LC batch up to 1.57 mm/mm2 for the blend with 0.2 wt-% Si powder.
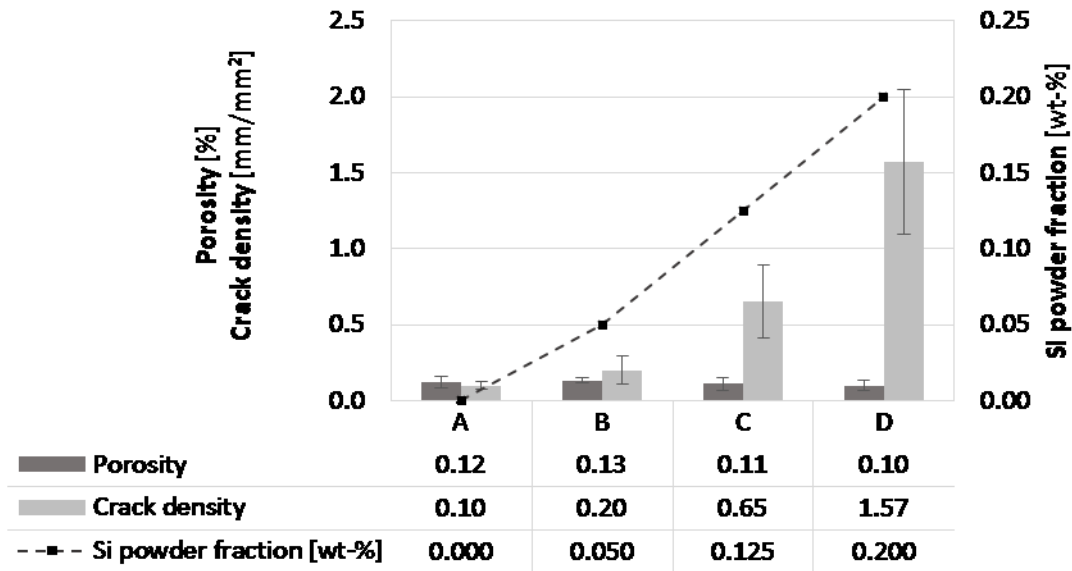
Figure 6: Results from quantitative image analysis of the xy-microsections. While the fraction of Si powder does not influence the porosity, a strong increase of the crack density can be observed with increasing Si powder fraction.

The microsections of the SLM processed samples made of pure IN738LC powder and the 0.2 wt-% Si powder blend was investigated by scanning electron microscopy. Figure 7 shows two BSE images of these microsections. The microstructure consists of small grains consisting of cells of around 1µm size and very fine carbides (bright spots in Figure 7) with a size considerably below 250nm. In both samples, some very fine pores are present (dark spots in Figure 7). However, no evidence for undissolved Si particles or Si enrichment could be observed.
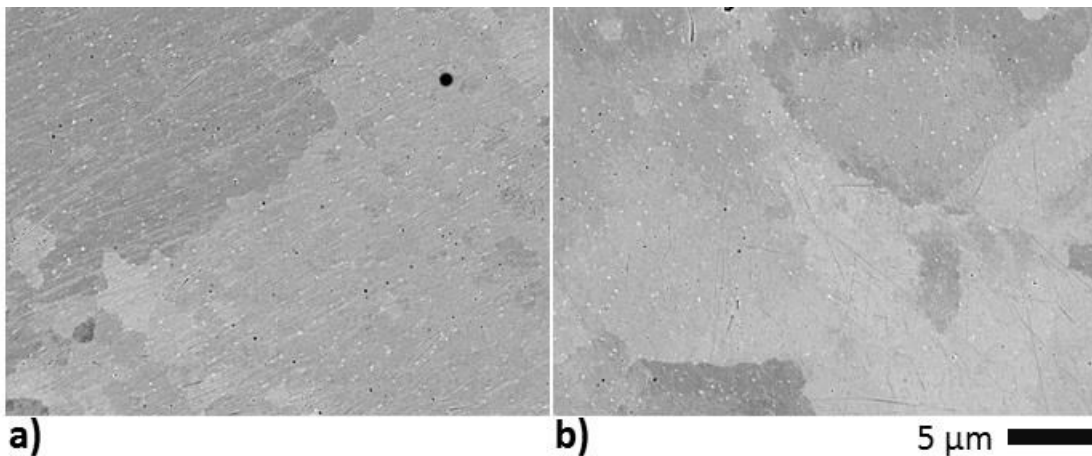

Figure 7: Backscatter electron images of polished microsections from SLM processed samples out of a) pure IN738LC powder and b) IN738LC powder blended with 0.2 wt-% Si powder. Fine pores (dark) and carbides (bright) can be seen in all samples, but no sign of remaining silicon particles or enrichment were observed. The contrast of the different areas in the images originates from channeling effects caused by slightly different orientations of the grains.

As Si is the only element whose concentration is changed significantly in the different blends (see Table 2), the present findings clearly show the detrimental effect of very small amount < 0.2 wt-% of Si in IN738LC on its SLM processability. In author's prior work [7], the crack densities of SLM processed specimens made from different gas atomized IN738LC powders varied between 0.3 and 3 mm/mm^2. Though the Si concentrations in the present work varied in a similar range, smaller variations in the crack densities were observed. However, it needs to be noted that these values are not directly comparable as the specimens of the present investigation were processed with different SLM equipment using a process parameter with considerably slower scan speed. For directionally solidified IN738LC, Zhu et al. [14] reported that the segregation of Si increases with increasing solidification rate from 12 mm/h to 50mm/h. If this trend also holds true for the much higher solidification rates present during SLM, it might contribute to the higher crack densities observed in the

author's prior work. Furthermore, those different batches varied in many elements simultaneously and the higher crack densities might also be caused by a synergistic effect of different detrimental elements.
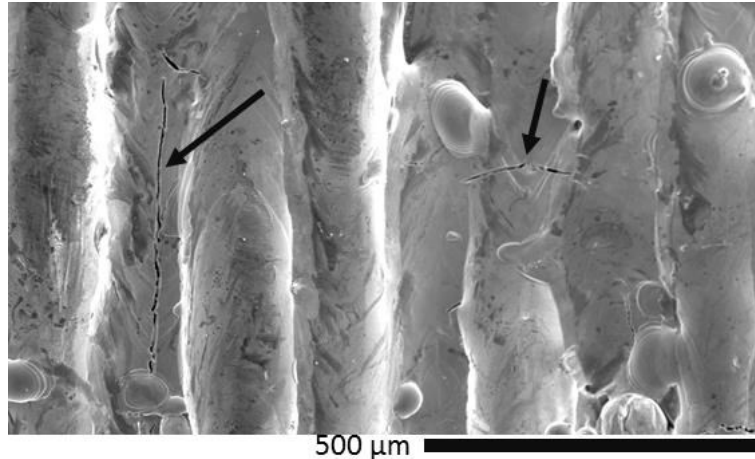

Figure 8: Secondary electron image of top surface from an SLM processed sample out of IN738LC with 0.2wt-% Si powder addition. As in the other samples, the cracks run both perpendicular and parallel to the scan line (see arrows).

All samples reveal cracks open to the top surface, which can run both along the scan line as well as perpendicular to the scan lines (see Figure 8). The SE images in Figure 9 show details of the fracture surface of the specimen made out of pure IN738LC powder. Large areas of the fracture surface exhibit dimple-like features as shown in image Figure 9a, characteristic for a ductile forced fracture. Figure 9b and Figure 9c show detail images of a crack running along and perpendicular to the scan vectors respectively. Both show rounded, cellular or dendrite like features characteristic for hot cracks forming under presence of a liquid phase [15].
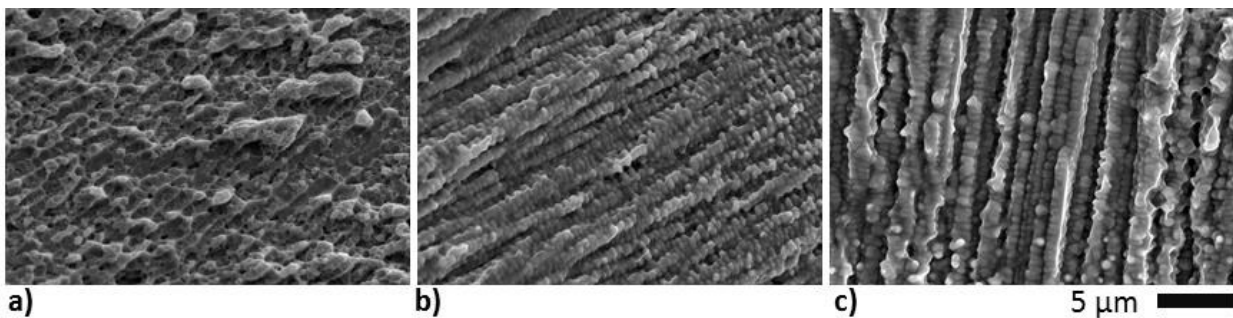

Figure 9: Secondary electron images of the crack surface from a broken open specimen processed out of IN738LC with no Si powder addition. a) Fracture surface showing dimples characteristic for a ductile forced fracture. b) Fracture surface of a hot crack perpendicular to the scan direction. c) Fracture surface of a hot crack running parallel in the center of the weld lines. The smooth, dendrite like features shown in b) and c) are typical for fractures occurring under presence of a liquid phase.
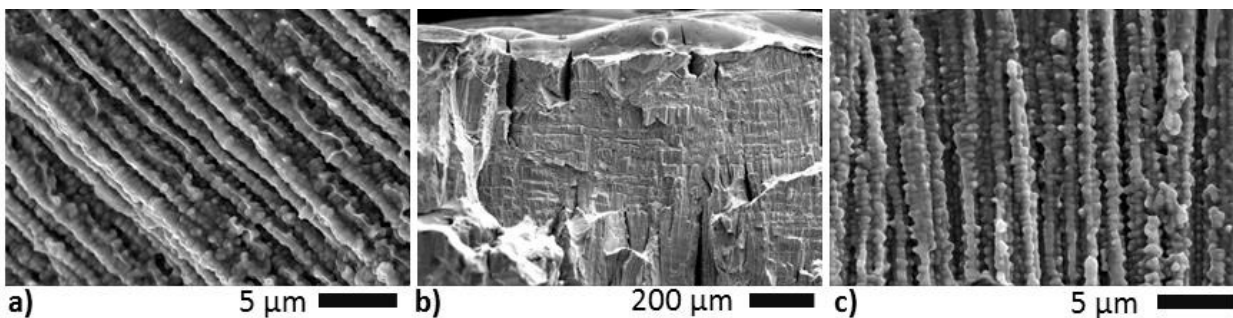

Figure 10: Secondary electron images of the crack surface from a broken open specimen processed out of IN738LC with 0.2wt-% Si powder addition. a) Fracture surface of a hot crack running perpendicular to the scan direction. b) View on a fracture surface running parallel to the scan lines. c) Close up of a hot crack running parallel to the scan lines. The smooth, dendrite like features shown are typical for fractures occurring under presence of a liquid phase.

The fracture surface of the specimen made out of the 0.2 wt-% powder blend shown in Figure 10 exhibits very similar features, but the area showing the hot crack features (Figure 10 a and c) almost covers the whole fracture surface. This can be well seen in the overview image (Figure 10b) looking on the fracture surface running parallel to the scan lines. The numerous cleavages in this fracture surface originate from crack running perpendicular to the scan vectors. The present investigation showed that cracks in as-built, SLM processed IN738LC are either solidification cracks, forming at the final stage of solidification, or liquation cracks, forming through liquation of segregated low-melting phases or constitutional liquation of precipitates during reheating by an adjacent scan line.

According Wolf [15], surfaces of solidification cracks typically show a pronounced columnar structure, whereas the structure on the surface of liquation cracks is more irregular. It is therefore expected that cracks in SLM processed IN738LC are more likely solidification cracks. This is supported by the fact that the cracks in the top layer are mostly open to the top surface and often run along the weld center line. Furthermore, only very fine precipitates are present in the as-built microstructure due to the very high cooling rates characteristic to the SLM process. As fine particles can dissolve faster upon heating, they are less likely to constitutional liquate as shown by Tancret [16] for liquation of γ` precipitations. Solidification cracking might be aggravated by segregation of Si to the interdendritic zone where it could result in an increased mushy zone as reported by Zhu et al. for casted IN738LC [14]. It is furthermore possible that Si affects the solid-liquid interface energy which could, according the work of Rappaz et al. [17,18], result in repulsive grain boundaries which also promote solidification cracking. Further investigations are ongoing to clarify the cracking mechanism observed with increasing Si content.

Summary & Outlook

Even in low concentrations below 0.2 wt-%, Si increases the alloy's tendency for hot cracking. The crack surfaces revealed that the cracks are formed under presence of a liquid phase, but the exact mechanism behind is not yet clear and requires further investigations.

The findings of the present work emphasize that alloy specifications optimized for SLM are necessary, especially if the process is to be industrialized. The creation of such a specification requires understanding of the influence of the different alloys on SLM processing. Based on the new findings, the IN738LC composition was optimized for the use for SLM (patent pending [19]) and is applied with good success to create parts with very low crack densities.

Acknowledgment

References

[1]   A. Gasser, G. Backes, I. Kelbassa, A. Weisheit, and K. Wissenbach, "Laser Additive Manufacturing," *Laser Technik Journal*, vol. 7, no. 2, pp. 58–63, Feb. 2010.

[2]   I. Kelbassa, P. Albus, J. Dietrich, and J. Wilkes, "Manufacture and repair of aero engine components using laser technology," in *Proceedings of the 3rd Pacific International Conference on Application of Lasers and Optics*, 2008, pp. 208–212.

[3]   E. Uhlmann and K. Urban, "Approach for the Qualification of Novel Materials for Selective Laser Melting for the Example of Nickel-base Superalloy Diamalloy4004NS," presented at the Direct Digital Manufacturing Conference, Berlin, 2012.

[4]   L. N. Carter, M. M. Attallah, and R. C. Reed, "Laser Powder Bed Fabrication of Nickel-Base Superalloys: Influence of Parameters; Characterisation, Quantification and Mitigation of Cracking," in *Proceedings of the Twelfth International Symposium on Superalloys*, 2012, pp. 577–586.

[5]   L. N. Carter, C. Martin, P. J. Withers, and M. M. Attallah, "The influence of the laser scan strategy on grain structure and cracking behaviour in SLM powder-bed fabricated nickel superalloy," *Journal of Alloys and Compounds*, vol. 615, pp. 338–347, Dezember 2014.

[6]   D. Tomus, T. Jarvis, X. Wu, J. Mei, P. Rometsch, E. Herny, J.-F. Rideau, and S. Vaillant, "Controlling the Microstructure of Hastelloy-X Components Manufactured by Selective Laser Melting," *Physics Procedia*, vol. 41, pp. 816–820, Jan. 2013.

[7]   R. Engeli, T. Etter, S. Hövel, and K. Wegener, "Processability of different IN738LC powder batches by selective laser melting," submitted to *Journal of Materials Processing Technology*

[8]   N. L. Richards and M. C. Chaturvedi, "Effect of minor elements on weldability of nickel base superalloys," *International Materials Reviews*, vol. 45, no. 3, pp. 109–129, Mar. 2000.

[9]   L. E. Rickenbacher, "Additive Reparaturstrategien für Strömungsmaschinenkomponenten," ETH Zürich, Zürich, 2012.

[10] C. A. Schneider, W. S. Rasband, and K. W. Eliceiri, "NIH Image to ImageJ: 25 years of image analysis," *Nature methods*, vol. 9, no. 7, pp. 671–675, 2012.

[11] X. He and J. Mazumder, "Transport phenomena during direct metal deposition," *Journal of Applied Physics*, vol. 101, no. 5, p. 053113, 2007.

[12] C. Panwisawas, C. L. Qiu, Y. Sovani, J. W. Brooks, M. M. Attallah, and H. C. Basoalto, "On the role of thermal fluid dynamics into the evolution of porosity during selective laser melting," *Scripta Materialia*, vol. 105, pp. 14–17, Aug. 2015.

[13] *Alloy IN-738 Technical Data*, vol. INCO Report 497. One New York Plaza, New York, USA: The International Nickel Company Inc., 1981.

[14] H. Q. Zhu, S. R. Guo, H. R. Guan, Y. X. Zhu, Z. Q. Hu, Y. Murata, and M. Morinaga, "The effect of silicon on the microstructure and segregation of directionally solidified IN738 superalloy," *Materials at high temperatures*, vol. 12, no. 4, pp. 285–291, 1994.

[15] M. Wolf, "Zur Phänomenologie der Heissrissbildung beim Schweissen und Entwicklung aussagekräftiger Prüfverfahren," Wirtschaftsverl. NW, Verl. für Neue Wiss., Bremerhaven, 2006.

[16] F. Tancret, "Thermo-Calc and Dictra simulation of constitutional liquation of gamma prime (γ') during welding of Ni base superalloys," *Computational Materials Science*, vol. 41, no. 1, pp. 13–19, Nov. 2007.

[17] M. Rappaz, A. Jacot, and W. J. Boettinger, "Last-stage solidification of alloys: Theoretical model of dendrite-arm and grain coalescence," *Metallurgical and Materials Transactions A*, vol. 34, no. 3, pp. 467–479, Mar. 2003.

[18] N. Wang, S. Mokadem, M. Rappaz, and W. Kurz, "Solidification cracking of superalloy single- and bi-crystals," *Acta Materialia*, vol. 52, no. 11, pp. 3173–3182, Jun. 2004.

[19] R. Engeli, T. Etter, and H. Meidani, "Gamma prime precipitation strengthened nickel-base superalloy for use in powder based additive manufacturing process," Patent EP2886225 (A1), 24-Jun-2015.